Human Molecular Genetics, 2014, Vol. 23, No. 10 **2604–2617**
doi:10.1093/hmg/ddt656
Advance Access published on December 23, 2013

Role of toll-like receptors in the pathogenesis of dystrophin-deficient skeletal and heart muscle

Andrea Henriques-Pons[1,4,†], Qing Yu[1,2,†], Sree Rayavarapu[1,3], Tatiana V. Cohen[1], Beryl Ampong[1], Hee Jae Cha[1], Vanessa Jahnke[1], Jack Van der Meulen[1], Daqing Wang[5], Weiwen Jiang[5], Ekambar R. Kandimalla[5], Sudhir Agrawal[5], Chistopher F. Spurney[1,2] and Kanneboyina Nagaraju[1,3,*]

[1]Center for Genetic Medicine Research, [2]Division of Cardiology, Children's National Medical Center, Children's Hospital, Washington, DC, USA, [3]Department of Integrative Systems Biology, The George Washington University, Washington, DC, USA, [4]Laboratório de Inovações em Terapias, Ensino e Bioprodutos, Fundação Oswaldo Cruz, Instituto Oswaldo Cruz, Rio de Janeiro, Brazil and [5]Idera Pharmaceuticals, Inc., Cambridge, MA, USA

Received September 16, 2013; Revised November 25, 2013; Accepted December 20, 2013

Although the cause of Duchenne muscular dystrophy (DMD) is known, the specific factors that initiate and perpetuate disease progression are not well understood. We hypothesized that leaky dystrophin-deficient skeletal muscle releases endogenous danger signals (TLR ligands), which bind to Toll-like receptors (TLRs) on muscle and immune cells and activate downstream processes that facilitate degeneration and regeneration in dystrophic skeletal muscle. Here, we demonstrate that dystrophin-deficient mouse muscle cells show increased expression of several cell-surface and endosomal TLRs. *In vitro* screening identified ssRNA as a relevant endogenous TLR7 ligand. TLR7 activation led to myd88-dependent production of pro-inflammatory cytokines in dystrophin-deficient muscle cells, and cause significant degeneration/regeneration *in vivo* in *mdx* mouse muscle. Also, knockout of the central TLR adaptor protein, myd88 in *mdx* mice significantly improved skeletal and cardiac muscle function. Likewise, proof-of-concept experiments showed that treating young *mdx* mice with a TLR7/9 antagonist significantly reduced skeletal muscle inflammation and increased muscle force, suggesting that blocking this pathway may have therapeutic potential for DMD.

INTRODUCTION

Duchenne muscular dystrophy (DMD) is an X-linked genetic disorder caused by loss-of-function mutations in the dystrophin gene. Dystrophin, a major component of the dystrophin glycoprotein complex (DGC) connecting cytoskeletal F-actin to the DGC and the extracellular matrix, is responsible for maintaining the integrity of skeletal and cardiac muscle fibers. Histopathological data in animal models and human DMD patients indicate that widespread necrosis of muscle fibers triggers a local inflammatory response that leads to additional secondary skeletal and cardiac tissue damage and fibrosis. We have previously demonstrated the up-regulated expression of both Toll-like receptor 7 (TLR7) and the adaptor molecule myeloid differentiation primary response gene 88 (myd88) in the skeletal muscle of DMD patients (1). More recently, we have also demonstrated that normal and dystrophin-deficient primary skeletal muscle cells are capable of secreting interleukin (IL)-1β in response to combined treatment with the TLR4 agonist lipopolysaccharide (LPS) and the P2X7 receptor agonist benzylated adenosine triphosphate, suggesting that both muscle cells and immune cells can actively participate in the inflammatory response (2).

Here, we tested the hypothesis that dystrophin-deficient cells undergoing necrosis may serve as a source of danger signals and trigger an immune inflammatory response by binding to and stimulating innate immune receptors, even in the absence of infection (the so-called 'danger model' of the immune response) (3,4). This response can activate intracellular signaling pathways, leading not only to an inflammatory response but also to many other effects on dystrophic skeletal muscle. Increasing

*To whom correspondence should be addressed at: Integrative Systems Biology and Pediatrics, Research Center for Genetic Medicine, Children's National Medical Center, 111 Michigan Avenue, N.W., Washington, DC 20010, USA. Tel: 1 202 4766220; Fax: +1 202 4766014; Email: knagaraju@cnmc.org
†Authors contributed equally.

evidence suggests that endogenous ligands released from damaged or stressed cells [damage-associated molecular patterns (DAMPs)] can stimulate TLRs and trigger an immune/inflammatory response. These signals can be generated when cells undergo pathological cell death (necrosis), as opposed to physiological apoptotic cell death, which does not trigger inflammation. However, 'stressed' or 'damaged' cells could generate signals in response to changes in the lipid and/or carbohydrate moieties expressed on their surfaces or by generating danger-sensing molecules that bind to either internal (e.g. TLR7, -8 and -9) or external (e.g. TLR4 and -2) receptors of the muscle and inflammatory cells in the milieu. TLRs associate with various cytoplasmic adaptor proteins, such as myd88, TIR-domain containing adapter-inducing interferon-ß, TRIF related adapter molecule and sterile alpha and armadillo motif containing protein. Myd88, a well-studied adaptor, is associated with all the TLRs except TLR3 (5).

In the present work, we demonstrate that *ex vivo* isolated MyoD$^+$ primary muscle cells from dystrophin-deficient *mdx* mice, a commonly used experimental model for DMD, express a variety of TLRs, and cultured primary myoblasts readily respond to both exogenous (LPS) and endogenous TLR7 ligand (ssRNA) by producing various cytokines. Further, injection of exogenous ssRNA induced muscle degeneration/regeneration in *mdx* mice. To address the role of TLRs *in vivo*, we produced dystrophin$^{-/-}$ (*mdx*)/myd88$^{-/-}$ double-deficient mice. At a young age, these *mdx*/myd88$^{-/-}$ mice showed no difference from age-matched *mdx*/myd88$^{+/+}$ mice in terms of regeneration, degeneration or inflammatory response. However, proliferation of the muscle cells was reduced *in vitro* and *in vivo* in the double-deficient mice. In older (1-year-old) mice, we detected improved skeletal muscle pathology, with less degeneration. Furthermore, cardiac function was improved in the older *mdx*/myd88$^{-/-}$ mice, with less degeneration and fibrosis than in *mdx*/myd88$^{+/+}$ mice. We also evaluated an antagonist of TLR7/9 signaling in the *mdx* mice (6). We found a significant reduction in skeletal muscle inflammation, degeneration and regeneration, demonstrating that the TLR 7/9 pathway is a potential therapeutic target in DMD.

RESULTS

TLRs are expressed in skeletal muscle cells

We have previously shown that TLR4 and TLR2 are expressed in MyoD$^+$ skeletal muscle cells (2). Here, we used flow cytometry to systematically assess the expression of several TLRs *ex vivo* in MyoD$^+$ muscle-committed progenitor cells from *mdx* dystrophic mice (Table 1). All the TLRs tested were evaluated in muscle cells isolated from soleus, gastrocnemius and diaphragm muscles, and the percentage of cells expressing a specific TLR in MyoD gated population was calculated. We found that the percentage of cells positive for a specific TLR varied within a muscle and also between muscle groups (Table 1). Muscle cells derived from the soleus, which is predominantly type 1, had more TLR expressing cells than the gastrocnemius, which is predominantly type 2. Muscle cells derived from the diaphragm showed a similar pattern as the soleus. Most cells in all three muscle types expressed TLR9 (Table 1).

Myoblasts produce cytokines in response to TLR ligands

We established primary cultures of myoblasts from the diaphragm, the most affected muscle in *mdx* mice, with a $\geq$95% enrichment of muscle-committed cells, as ascertained by desmin immunostaining (Fig. 1A and B). Prior to incubation with the agonists, we ensured that there was no detectable cell death in these cultures (i.e. no TUNEL$^+$ cells), which would lead to the release of endogenous DAMPs (data not shown). Third-passage (P3) cultures were then exposed to various concentrations of LPS (positive control) or the endotoxin-free endogenous TLR ligands HMGB1, hyaluronic acid fragments (all TLR4 ligands) and ssRNA (TLR7 ligand-internalized through endocytosis), and the supernatants were evaluated for various cytokines by flow cytometry. Treatment with ssRNA (6 μg/ml) induced a ~200-fold increase in TNF-α expression (Fig. 1C), ~2-fold increase in IL-6 expression (Fig. 1D) and ~5-fold increase in MCP-1 expression (Fig. 1E), but did not affect IL-10 expression (Fig. 1F) when compared with untreated cells (negative control) (Supplementary Material, Table S1). We did not observe any detectable secretion of IL-12p70 or IFN-γ at the ligand dosages tested (data not shown). When we used 3 μg/ml of ssRNA, we found a ~80-fold increase in TNF-α (Fig. 1C) and 4-fold increase in MCP-1 (Fig. 1E) (Supplementary Material, Table S1). LPS induced high levels of TNF-α, IL-6, MCP-1 and IL-10 secretion (Fig. 1C–F), but not IL-12p70 or IFN-γ (data not shown). The other ligands, hyaluronic acid fragments and HMGB1 did not induce the production of any of the cytokines tested in our system (Fig. 1C–F). Under these conditions, the agonists did not induce myoblast differentiation or cell death (data not shown).

The TLR7 ligand ssRNA induces muscle inflammation in *mdx* mice

Since ssRNA induced a robust cytokine response *in vitro* in primary muscle cells, we decided to test its effect *in vivo* in the quadriceps of 2-month-old *mdx* mice. Histological analysis for inflammation, regeneration and degeneration by hematoxylin & eosin (H&E) staining showed no significant infiltration in C57BL/10 or *mdx* mice that had been treated with saline

Table 1. TLR expression in MyoD$^+$ muscle cells from mdx mice

Muscle type	TLR1	TLR2	TLR3	TLR4	TLR7	TLR8	TLR9
Gastrocnemius[a]	22.6	60.9	37.1	42.0	28.2	46.1	95.2
Soleus[a]	83.6	87.2	98.0	74.8	99.1	86.4	97.3
Diaphragm[a]	86.4	65.8	94.3	75.2	97.4	87.7	97.4

[a]Percentage of TLR expression in the gated MyoD$^+$ cells.

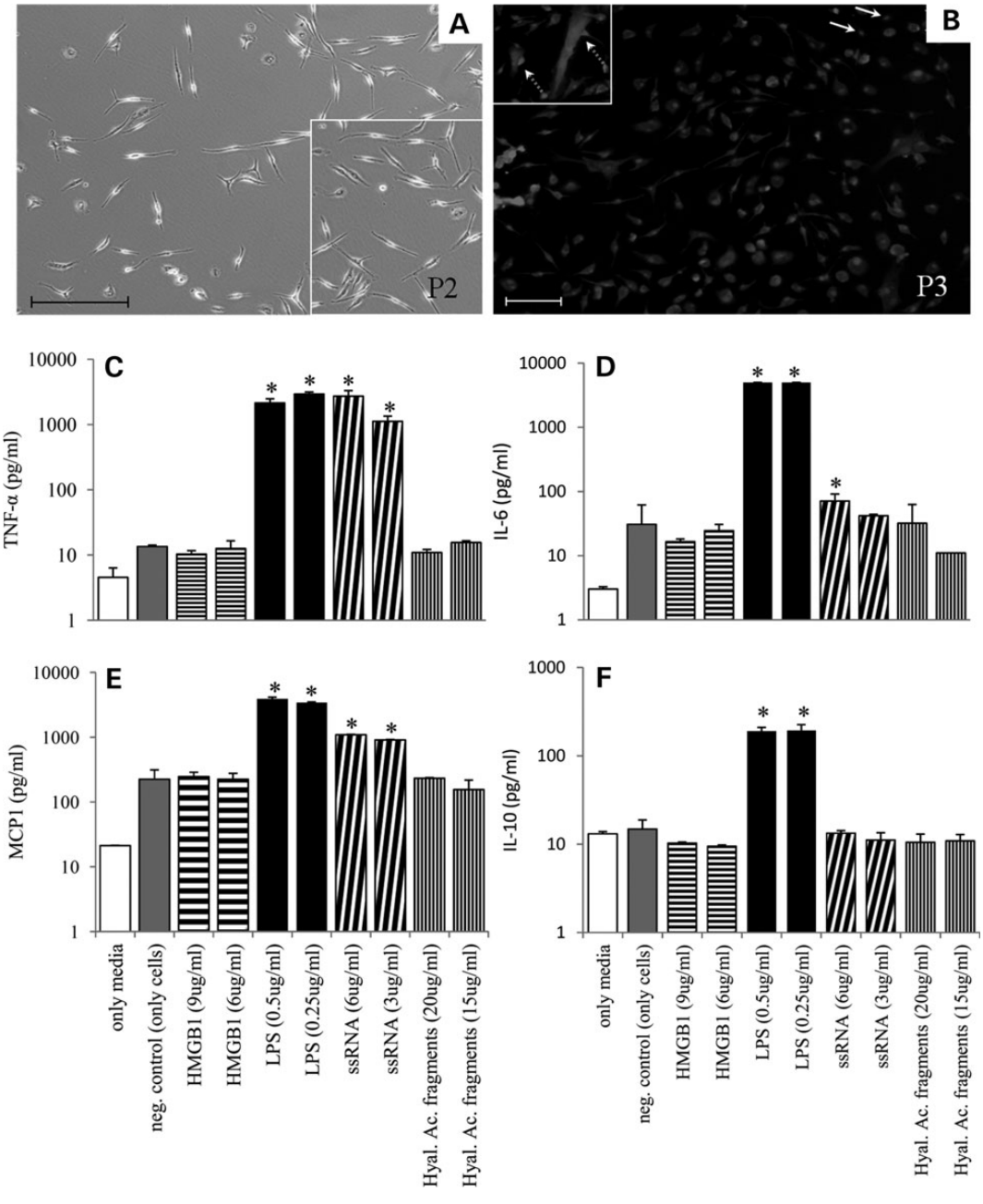

Figure 1. Myoblast cultures and stimulation by TLR agonists: myoblast cultures were obtained from diaphragm fragments from 2-month-old *mdx* mice, here shown in the second passage (P2) (**A**), with at least 95% enrichment of desmin-positive muscle-committed cells in P3 (**B**). At this stage, the cells were exposed for 18 h to the indicated concentrations of HMGB1, lipopolysaccharide (LPS), ssRNA or hyaluronic acid fragments as TLR ligands. The levels of TNF-α (**C**), IL-6 (**D**), monocyte chemoattractant protein -1 (MCP1) (**E**) and IL-10 (**F**) were then evaluated by flow cytometry in culture supernatants using a commercial kit (CBA flex). Nuclear labeling was done using DAPI. $^{*}P \leq 0.05$ when compared with the negative control (cells only, with no agonist). Arrows indicate desmin-negative cells, and dashed arrows indicate myoblasts fusing. Bar = 50 μm. Three independent experiments were done, and a representative result is shown.

(Supplementary Material, Fig. S1A and B). However, LPS injections induced a strong mononuclear cell infiltration in both mouse strains, and the inflammatory response was much stronger in the *mdx* mice (Supplementary Material, Fig. S1C and D). Injection of ssRNA (9 μg/ml) caused no inflammatory infiltration in the C57BL/10 mice (Supplementary Material, Fig. S1E) and produced only a mild inflammatory foci around the site of injection in the *mdx* mice (Supplementary Material, Fig. S1F). Injection of 12 μg/ml of ssRNA also caused only a mild inflammatory reaction in the C57BL/10 mice (Supplementary Material, Fig. S1G); however, the same concentration (12 μg/ml) of ssRNA induced a strong local inflammatory response in the *mdx* mice (Supplementary Material, Fig. S1H).

We then stained muscle sections with anti-embryonic myosin heavy chain (eMHC) to look for regeneration (strongly positive cells) and degeneration after TLR ligand treatment. Degenerating fibers were identified as having diffuse and pale staining with indistinct cytoplasmic structures or sarcolemma. We did not

observe eMHC$^+$ cells in the C57BL/10 mice treated with saline (Fig. 2A and I), but a few regenerating cells were found in *mdx* mice (Fig. 2B and J). No degeneration was seen in either group of mice (Fig. 2A, B, I and J). However, C57BL/10 mice treated with LPS showed a significant number of degenerating fibers (Fig. 2C and I) and very few eMHC$^+$ regenerating cells (Fig. 2C and I). LPS-treated *mdx* mice showed higher levels of both degenerating and regenerating muscle cells (Fig. 2D and J). When we used ssRNA at 9 μg/ml, we observed no eMHC$^+$ cells in C57BL/10 mice (Fig. 2E and I), but regeneration in *mdx* reached as high as 40% on average (Fig. 2F and J). Although the highest dose of ssRNA induced some regeneration in C57BL/10 mice (Fig. 2G and I), it induced significant degeneration and regeneration in the *mdx* mice (Fig. 2H and J). These changes in inflammation, degeneration and regeneration were always observed close to the point of needle insertion, with the injection scar visible in some panels of Figure 2.

Mdx/myd88$^{-/-}$ muscle cells show decreased cytokine secretion and reduced cell proliferation

To ascertain whether the ssRNA-induced cytokine secretion in skeletal muscle cells was myd88 dependent, we isolated muscle cells (diaphragm) from *mdx*/myd88$^{+/+}$ and *mdx*/myd88$^{-/-}$ mice (Supplementary Material, Fig. S2), then plated total muscle cells and incubated them in the presence of TLR ligands for 18 h. Muscle cells from *mdx*/myd88$^{+/+}$ mice that were incubated with LPS or ssRNA secreted high levels of TNF-α (Fig. 3A), monocyte chemoattractant protein -1 (MCP1) (Fig. 3B) and IL-6 (Fig. 3C), when compared with untreated controls. We did not detect significant cytokine secretion in response to stimulation with hyaluronic acid fragments (Fig. 3A–C). However, muscle cells from *mdx*/myd88$^{-/-}$ mice showed a marked decrease in TNF-α and IL-6 (but not MCP-1) secretion in response to LPS stimulation, when compared with *mdx*/myd88$^{+/+}$ cells (Fig. 3A–F). In contrast, the ability of ssRNA to induce cytokine secretion was completely abrogated in the cells from *mdx*/myd88$^{-/-}$ mice (Fig. 3D–F), suggesting that the cytokine response to TLR7 is dependent on myd88 in skeletal muscle cells. We did not detect any cytokine secretion in response to hyaluronic acid fragments, nor did we see any detectable levels of IL-10, IL-12p70 or IFN-γ in either group of mice (data not shown).

To determine the proliferative ability of *mdx*/myd88$^{-/-}$ double-deficient muscle *in vivo*, we treated these mice with BrdU and counted the positive muscle cells by flow cytometry. The double-deficient mice showed fewer BrdU-positive cells than the *mdx*/myd88$^{+/+}$ mice (Fig. 4A). These findings were further corroborated by Ki67/MyoD and MyoD/Pax7 double staining of skeletal muscle. The *mdx*/myd88$^{-/-}$ mice showed a significant reduction in double-positive cells (Fig. 4B and C) in the diaphragm and gastrocnemius muscles. We also found that general proliferation of cells in the diaphragm and gastrocnemius slices was significantly decreased in the *mdx*/myd88$^{-/-}$ mice (Fig. 4D).

mdx/myd88$^{-/-}$ mice show an improved skeletal muscle phenotype

We have systematically evaluated the phenotype of double-deficient mice up to 12 months of age using a standardized set of behavioral and functional assessments. The *mdx*/myd88$^{-/-}$ mice showed improved normalized hindlimb grip strength and specific force in the extensor digitorum longus (EDL) muscle when compared with *mdx*/myd88$^{+/+}$ mice (Fig. 5B and C). However, we saw no significant differences in motor coordination or open-field behavioral activity measures (data not shown).

To assess the effect of myd88 deficiency on the skeletal muscle phenotype, we evaluated H&E sections of gastrocnemius and diaphragm muscle from young (2–4 months of age) *mdx*/myd88$^{+/+}$ and *mdx*/myd88$^{-/-}$ mice. We did not detect any histological differences in muscle inflammation, regeneration or degeneration at this age (data not shown). Moreover, there were no differences in MyoD or myogenin differentiation cell markers, which are associated with the early and late stages of muscle regeneration, as assessed by either histological (Supplementary Material, Fig. S3A–F) or immunoblotting analyses of the diaphragm and gastrocnemius extracts from 2 to 4-month-old mice (Supplementary Material, Fig. S3G). On the other hand, when we evaluated IgM labeling (a marker of degeneration) in 12-month-old mice, we observed significantly less degeneration in the diaphragm and heart muscle (but not in gastrocnemius) of *mdx*/myd88$^{-/-}$ mice than in age-matched *mdx*/myd88$^{+/+}$ mice (Fig. 5A). Furthermore, *mdx*/myd88$^{-/-}$ mice showed significantly reduced serum CK levels at this age when compared with *mdx*/myd88$^{+/+}$ mice (Fig. 5D).

mdx/myd88$^{-/-}$ mice show improved cardiac phenotype

Because the cardiac dystrophy phenotype is apparent in *mdx* mice older than 9 months, we evaluated cardiac fibrosis and function in 10–12-month-old mice. Staining of cardiac tissue sections with Sirius red showed no fibrosis in controls (Fig. 6A and D), but large areas of collagen deposition in *mdx*/myd88$^{+/+}$ mice (Fig. 6B and D). However, we observed about half as much fibrosis in the *mdx*/myd88$^{-/-}$ mice (Fig. 6C and D) as in *mdx*/myd88$^{+/+}$. Also, *mdx*/myd88$^{-/-}$ mice showed improved cardiac function in terms of endocardial ejection fraction (EF), endocardial fractional area change (FAC), M-mode LV fractional shortening (FS) and M-lode LV EF when compared with *mdx*/myd88$^{+/+}$ mice (Table 2). We did not detect differences in the heart rate (bpm) in any of the groups tested (Table 2). Both *mdx*/myd88$^{+/+}$ and *mdx*/myd88$^{-/-}$ mice showed reduced aortic maximal velocity and aortic velocity time when compared with the control group (Table 2).

Blocking TLR7/9 signaling improves the disease phenotype in mdx mice

Treatment of *mdx* mice with the TLR7/8/9 antagonist for 4 weeks, starting at 5 weeks of age, resulted in a significant reduction in muscle inflammation, as revealed by optical imaging analysis of cathepsin activity (Fig. 7A) and levels of serum creatine kinase (Fig. 7B). *In vitro* force assessments of EDL muscle showed no statistically significant difference, but there was a trend toward improvement when compared with vehicle-treated *mdx* mice (Fig. 7C). H&E evaluation of skeletal muscle indicated a significant decrease in inflammation after treatment with the TLR antagonist (Fig. 7D). Furthermore, a significant

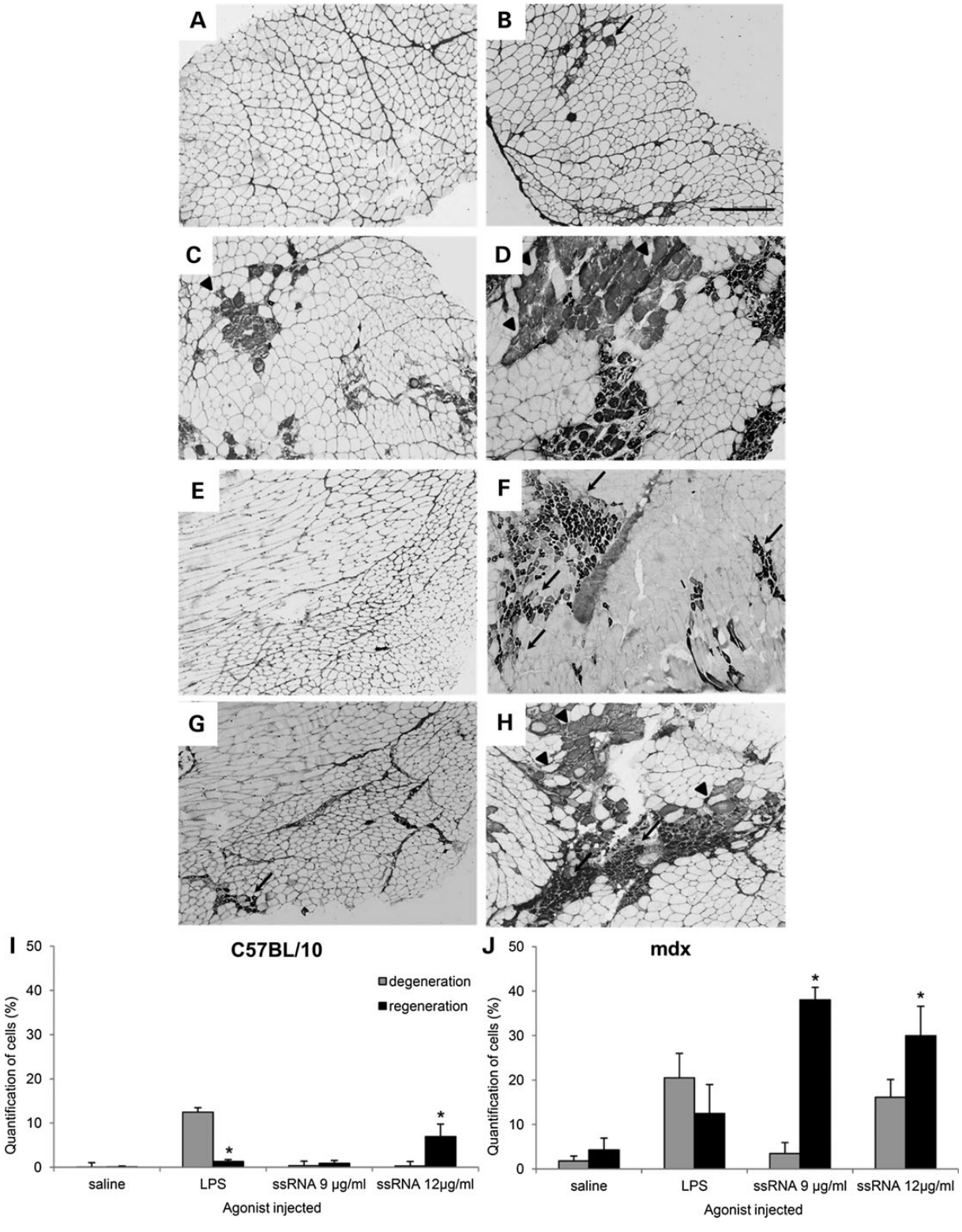

Figure 2. Muscle cell regeneration after *in vivo* intramuscular injection of TLR ligands: All C57BL/10 (left panels) and *mdx* (right panels) mice received injections of saline three times in the left quadriceps (four injections of 10 μl per muscle each time) at intervals of 3 days (**A** and **B**). The contralateral muscle received, in parallel, the same treatment of 2 μg/ml LPS (**C** and **D**), 9 μg/ml ssRNA (**E** and **F**) and 12 μg/ml ssRNA (**G** and **H**). Three days after the last injection, the mice were sacrificed, and all samples were collected and immunostained with anti-eMHC. Arrows indicate positive cells, and arrowheads indicate degenerating myofibers. Quantitation of regeneration and degeneration in *mdx* mice treated with TLR agonists was based on the labeling of anti-eMHC in C57BL/10 (**I**) or *mdx* (**J**) mice. We quantified the number of darkly positive cells (regeneration) and all cells per microscopic field in tissue slices and expressed the data as the percentage of positive cells. Lightly positive cells with blurred labeling and no distinguishable intracellular structures or sarcolemma were considered degenerating muscle fibers. Each group consisted of five mice, and the results shown are representative of two independent experiments (Bar = 200 μm). The quantitative analysis was done in at least 60 microscopic fields from three mice per group. $^{*}P \leq 0.05$ compared with the saline group in each mouse strain.

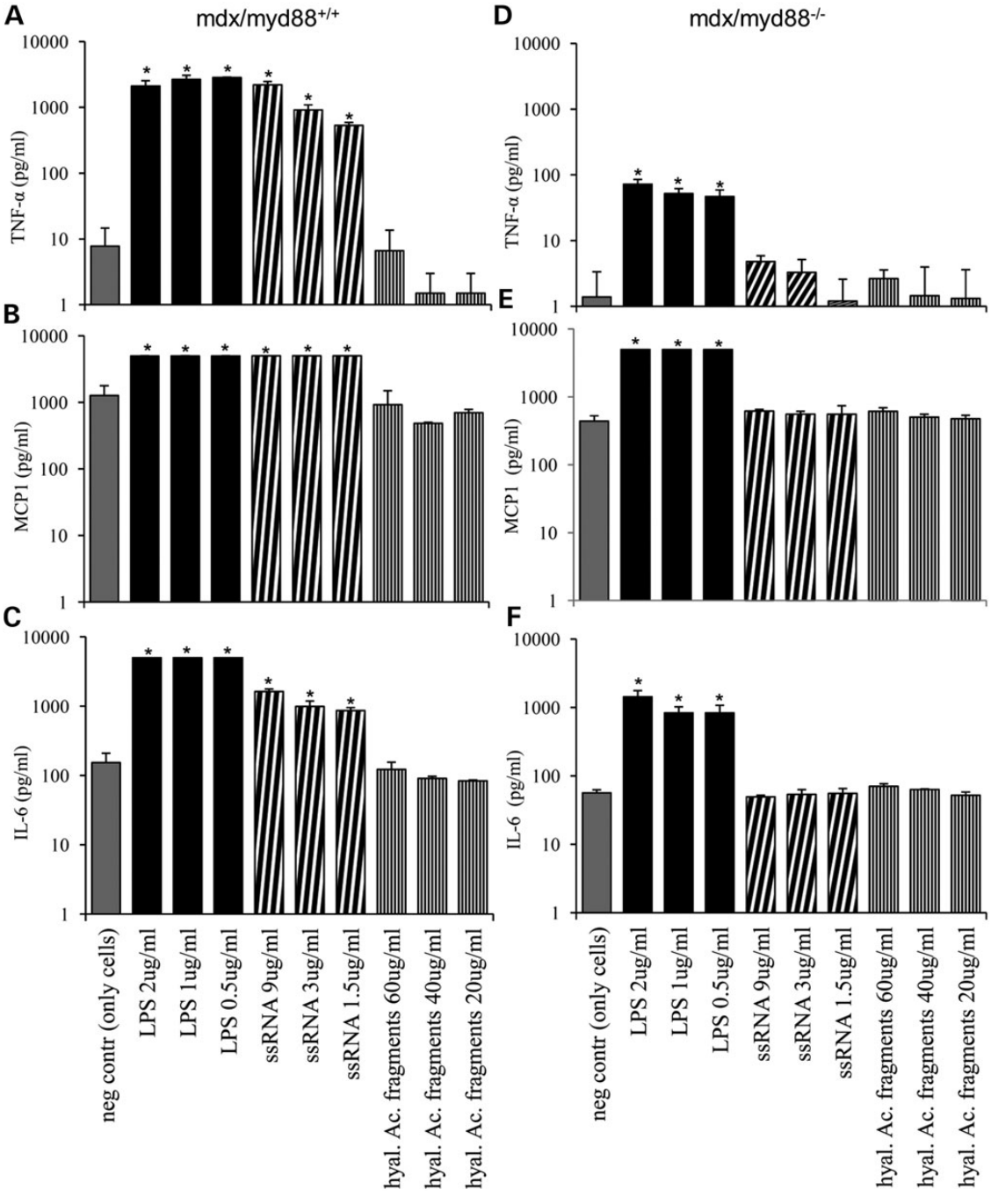

Figure 3. Myd88-dependent cytokine secretion by muscle cells: diaphragm muscles from *mdx*/myd88$^{+/+}$ (left panels) and *mdx*/myd88$^{-/-}$ (right panels) mice were plated and maintained in culture for 24 h. All supernatants were removed for incubation with agonist at the indicated concentrations. After 18 h of incubation, we measured the concentration of TNF-α (**A** and **D**), MCP1 (**B** and **E**) and IL-6 (**C** and **F**) using a CBA flex kit for flow cytometry. Data are expressed as picograms/mililiter, with a maximal detection level of 5000 pg/ml (due to the standard curve limit). $^{*}P \leq 0.05$ when compared with the negative controls (only cells).

reduction in the gene expression of the inflammatory cytokine (IFN-γ) was observed in the treated *mdx* mice (Fig. 7E). Other inflammatory markers such as TNF-α, TGF-β and IL-1β showed no decrease in expression (Fig. 7F–H). Taken together, these data suggest that blocking TLR7/9-mediated inflammatory pathways halts the degeneration/regeneration cycles in dystrophin-deficient muscle.

DISCUSSION

In this paper, we have shown that skeletal muscle cells express TLRs that respond to potential endogenous ligands and produce pro-inflammatory cytokines, which in turn initiate and perpetuate an inflammatory response in dystrophin-deficient skeletal muscle. We also showed that the TLR signaling in

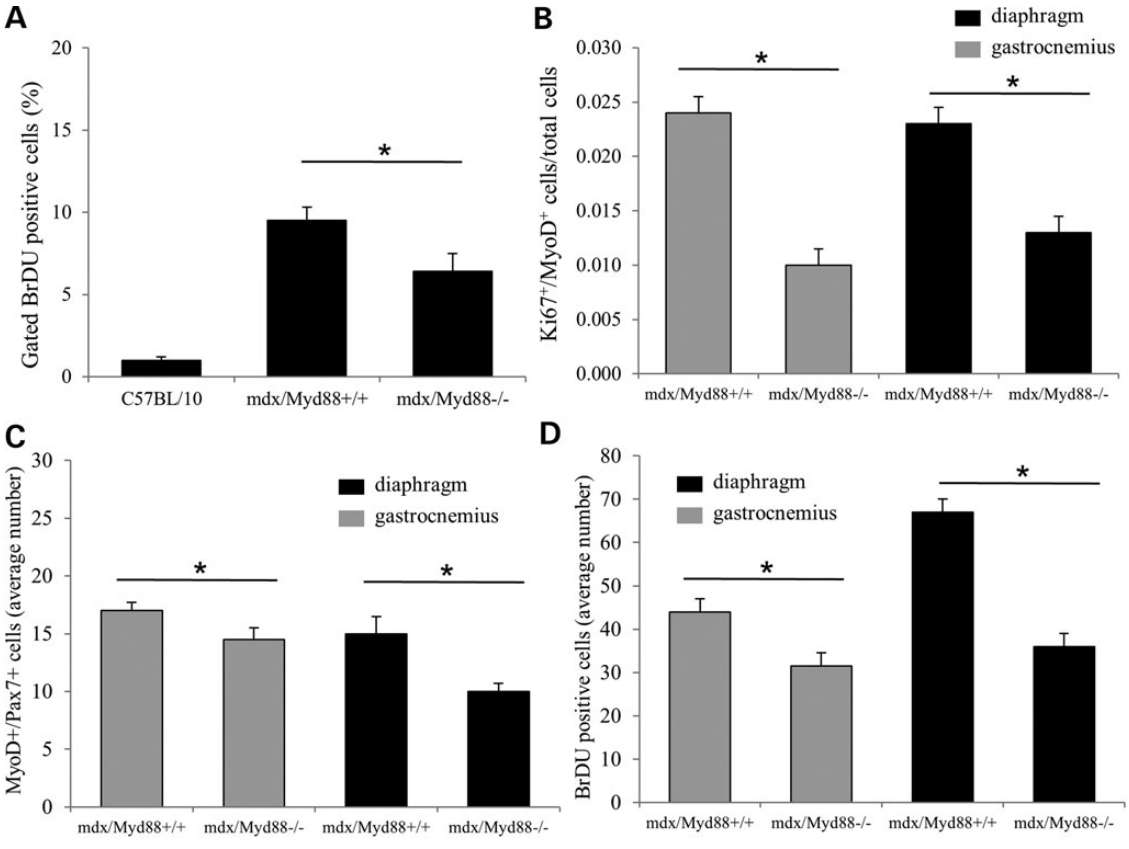

Figure 4. Proliferation of muscle cells from *mdx*/myd88$^{-/-}$ mice: all mice were treated with BrdU administered in the drinking water, and the gastrocnemius muscles from the indicated mouse lineages were dissociated using collagenase and analyzed by flow cytometry (**A**). To analyze the proliferation of muscle subpopulations, we labeled diaphragm and gastrocnemius slices with anti-Ki67 and anti-MyoD (double-positive cells considered proliferating myoblasts) (**B**) and with anti-Pax7 and anti-MyoD (double-positive cells considered satellite cells in self-renewal cycle) (**C**). The average number of BrdU-positive cells in diaphragm and gastrocnemius of each strain measured were shown (**D**). BrdU-positive and immunophenotyped cells in the diaphragm and gastrocnemius were individually counted in six sections in three mice per group. $^{*}P < 0.05$ when compared between *mdx*/myd88$^{+/+}$ and *mdx*/myd88$^{-/-}$ mice.

muscle cells is dependent on the TLR adaptor protein myd88 and that mice doubly-deficient in dystrophin and myd88 have a milder disease phenotype and improved cardiac function. We further showed that treating young *mdx* mice with a TLR7/9 antagonist significantly reduces inflammation, serum CK levels and improves skeletal muscle pathology.

We have previously demonstrated that DMD muscle biopsies display a significant mononuclear cell infiltration, and many of the infiltrating cells expressed immature (CD86 and human leukocyte antigen-DR) and mature (dendritic cell-lysosomal associated membrane protein) dendritic cell markers. Analysis of the gene expression profiles of biopsies from DMD patients also showed significant increases in the expression of TLR2, TLR7 and the major adaptor protein myd88 when compared the controls. DMD biopsies showed intense TLR7 staining in both the muscle fibers and the infiltrating mononuclear cells, as well as enhanced expression of several downstream classical NF-κB target genes (e.g. β2m and vimentin), including MHC class I alleles, suggesting that the TLR pathway is highly activated in DMD patients (1).

It is known that endogenous molecules such as hsp60 could stimulate TLR4-dependent cytokine secretion (7). Here, we have tested the hypothesis that endogenous danger signals engage TLRs and influence the muscle microenvironment in dystrophin-deficient skeletal muscle. We observed that freshly collected MyoD^{+} muscle cells expressed a broad panel of TLRs and responded to DAMPs and LPS *in vitro* by secreting pro-inflammatory cytokines. We have used explants to isolate primary myoblasts instead of crude enzymatic digestion preparations that are generally used to isolate primary myoblasts in order to avoid excess cell death and release of endogenous TLR ligands.

The proportion of muscle cells expressing TLRs varied between the three muscle types that we have tested. Muscle pathology in DMD is generally more in fast twitch than slow twitch muscle; however, expression of TLRs did not correlate with the pathology, suggesting that the presence of individual TLRs in a specific muscle may or may not directly correlate with extent of damage. One of the reasons could be that TLR expression was done on isolated cells, making it difficult to know the origin of these myoblasts because both muscle types have mixed fiber typing (gastrocnemius-predominantly type-2 and soleus-predominantly type-1). Therefore, enhanced expression of TLRs does not directly mean more muscle damage, but likely higher cytokine/chemokine secretion and inflammatory response.

Despite the presence of different TLRs, only some ligands induced a cytokine response. For example, LPS induced all the cytokines tested, whereas HMGB1 induced none of them, and the others such as ssRNA triggered the production of cytokines

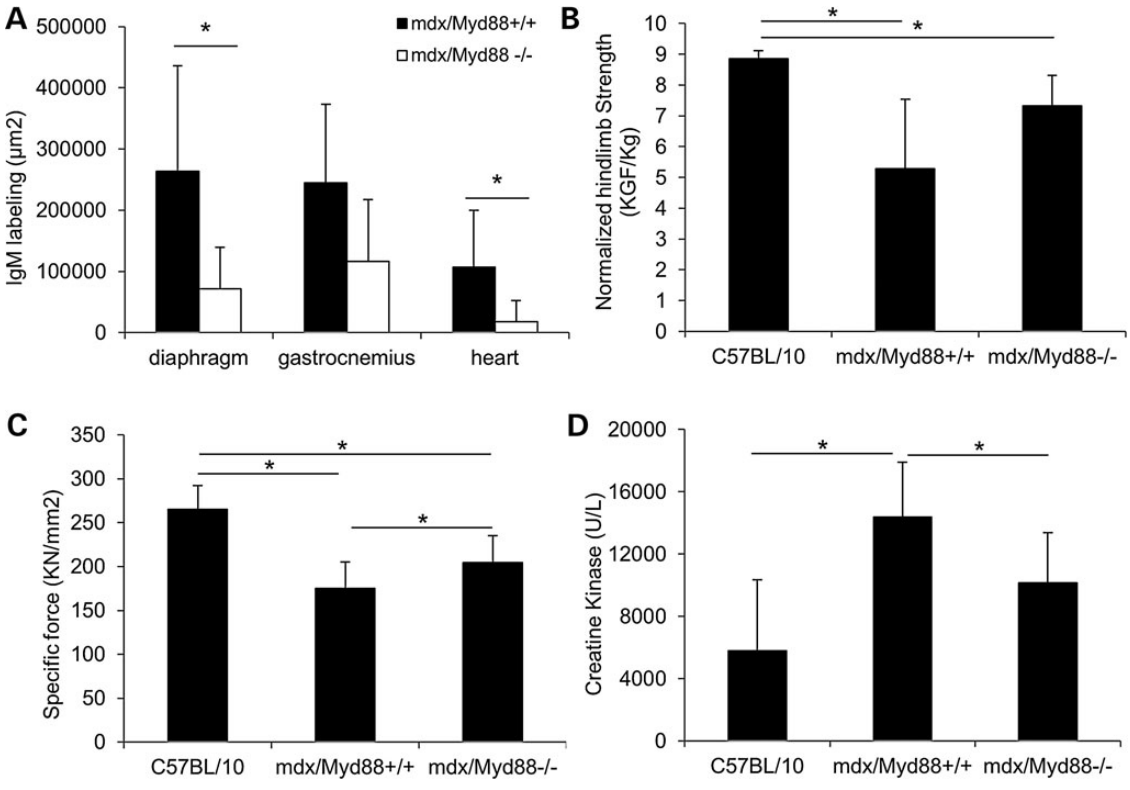

Figure 5. Dystrophinopathy in *mdx*/myd88$^{-/-}$ mice: (**A**) degenerating cells evaluated by IgM labeling, measuring the stained area in relation to the whole area of the tissue in the diaphragm, gastrocnemius and heart. (**B**) Hind limb grip strength normalized to bodyweight was shown. (**C** and **D**) Specific force of the EDL muscle (C) and serum CK levels (used as a marker of skeletal muscle damage) (D) were shown. Data are presented as mean ± SD for five mice per group ($^{*}P < 0.05$ by Students *t*-test).

such as TNF-alpha and MCP1. It is known that ssRNA signals through TLR7 and 8, while HMGB1 signals through TLR2 and probably TLR4 (in this case requiring MD-2 and CD14). Hyaluronic acid fragments may also signal through TLR2 and TLR4, possibly requiring CD44, and LPS requires LPS-binding protein (LBP), MD-2, TLR4 and CD14. This suggests that a response to a particular ligand is dependent not only on specific TLR expression but also on the presence several other co-associated molecules in a tissue, thus contributing to a differential cytokine response. Production of cytokines such as TNF-α and MCP1 by muscle cells in response to a TLR7 agonist indicates a role for muscle-derived cytokines and chemokines not only in attracting and activating macrophages and initiating inflammatory process but also in affecting myogenesis at the injured site (8,9). We have further demonstrated that TLR7-dependent cytokine secretion in skeletal muscle cells is myd88 dependent.

Although DAMPs and PAMPs bind to the same receptors, they may not all share the same molecular requirements at the cellular level and produce similar effects. For example, *in vivo* injection of LPS induced the migration of inflammatory cells in C57BL/10 and *mdx* mice, with a stronger response in the dystrophic mice. However, ssRNA injection induced an inflammatory response only in the *mdx* mice and not in the C57BL/10 mice. Thus, C57BL/10 mice responded to a PAMP but not to a DAMP. This failure to respond to the DAMP could be the result of a lack of the necessary repertoire of accessory and adaptor molecules required for this DAMP. Other accessory factors may be required to trigger an inflammatory response in muscle. It is also possible that the preexisting inflammatory microenvironment found in the mdx mice prompted a stronger response after the ssRNA injection, which was not seen in the C57BL/10 mice after the ssRNA treatment. The threshold for activation in dystrophin-deficient skeletal muscle may be lower because of the sustained contraction-induced injury that this tissue undergoes in the absence of dystrophin.

Although the injection of ssRNA into *mdx* mice led to local inflammatory responses as well as degeneration and regeneration, the natural course of the dystrophinopathy in *mdx*/myd88$^{-/-}$ mice showed no differences in these parameters from young age-matched *mdx*/myd88$^{+/+}$ mice. These data indicate that absence of TLR signaling in double-deficient mice lead to upregulation of other innate immune pathways that override the beneficial effects of TLR signaling. Also the changes observed after ssRNA injections are in a small area around injection site and may not reflect overall change in markers of regeneration (MyoD or myogenin) as assessed in whole muscle extracts by western blotting analysis or H&E evaluation of muscle section. In mdx mice muscle degeneration and regeneration occurs in cycles, more prominently in early age and at lower pace in later stages. Skeletal muscle and cardiac beneficial effects seen in older double-deficient mice suggest that blocking of TLR pathways from birth would have significant beneficial effects in older age as reflected in increased cardiac function and decreased fibrosis.

In *mdx* mice, we showed that both LPS and the higher dose of injected ssRNA-induced inflammatory cell infiltration. When

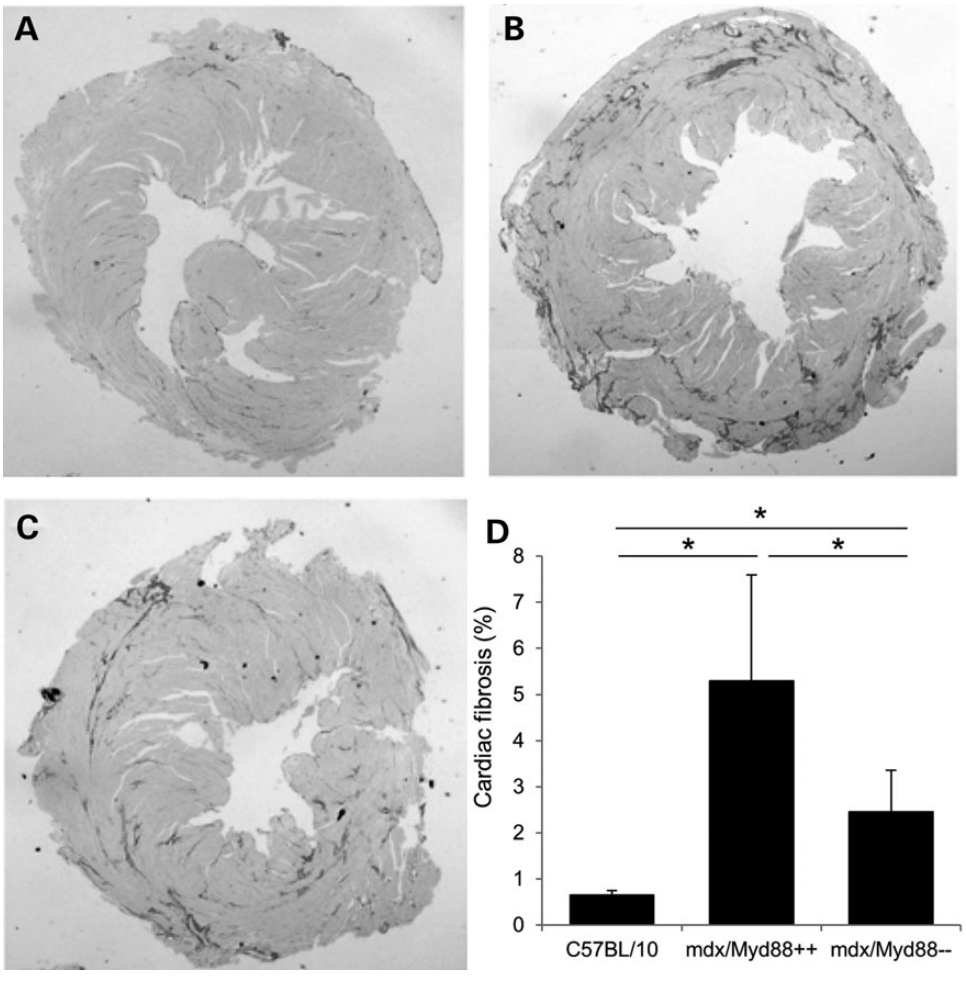

Figure 6. Cardiac fibrosis: cardiac tissue sections were collected from 10- to 12-month-old C57BL10 controls (**A**), *mdx*/myd88$^{+/+}$ mice (**B**) or *mdx*/myd88$^{-/-}$ mice (**C**). The slices were paraffin-embedded, cut and stained with picrosirius red. (**D**) Quantitation of fibrosis was done by measuring the positive areas stained with picrosirius red in relation to the whole area of the slice, and the results were expressed as percent collagen deposition. The mdx/myd88$^{-/-}$ mice showed significantly ($^{*}P < 0.05$) decreased fibrosis when compared with mdx/myd88$^{+/+}$ mice (**D**).

we injected the ssRNA, we observed degenerating fibers in both mouse lineages, but strongly positive eMHC cells (regeneration) were frequently observed only in *mdx* mice. Moreover, in the C57BL/10 mice, ssRNA induced few eMHC-positive cells at any concentration tested, whereas the muscle of the *mdx* mice was prompted to respond to this DAMP. In the absence of any significant death of muscle fibers, we observed that the ssRNA (9 μg/ml) injected *in vivo* into the *mdx* mice induced regeneration of new muscle cells. To our knowledge, this is the first time that *in vivo* exposure to a DAMP has been shown to trigger progenitor cell differentiation in dystrophic skeletal muscle. This finding may be important for future therapeutic strategies, regardless of the progenitor population targeted.

The myd88 adaptor molecule participates in the signal transduction pathways of all the TLRs, except TLR3, and the IL-1R and IL-18R signaling pathways. Because of its predominant pro-inflammatory role, we expected to find a decrease in the inflammatory response in the skeletal muscle of young *mdx*/myd88$^{-/-}$ mice. It is possible that the lack of overt histological improvements during acute necrotic phase in double-deficient mice could be because of the overwhelming nature of muscle necrosis that induces not only TLR but several other inflammatory and cell death processes that are activated in a myd88-independent manner.

Our data indicate that there is an improvement in cardiac function and a lower degree of cardiac fibrosis in older *mdx*/myd88$^{-/-}$ than in *mdx*/myd88$^{+/+}$ mice. These data are in agreement with recent reports showing that DAMP-dependent or -independent TLR signaling through myd88 leads to cardiomyocyte dysfunction and heart failure (10). In an inflammatory model, induction of myocarditis in wild-type and myd88$^{-/-}$ mice and injection of an irritant such as complete Freund's adjuvant promote cardiac fibrosis, ventricular dilation and impaired heart function only in wild-type but not myd88$^{-/-}$ mice suggesting a role in left ventricular hypertrophy and cardiac fibrosis (11). Pharmacologic inhibition of myd88 and myd88-targeted siRNA can protect against left ventricular dilatation and hypertrophy after infarction (12).

Since this pathway is amenable for therapeutic intervention Idera Pharmaceuticals has developed oligonucleotides that contain 2′-*O*-methyl-ribonucleotide substitutions; these oligonucleotides do not induce immune responses in mice, but they

Table 2. Cardiac function by echocardiography

Parameter	C57BL/10	*mdx/myd88*$^{+/+}$	mdx/myd88$^{-/-}$
Heart Rate (bpm)	469 ± 9	455 ± 16	478 ± 17
Aortic Maximal Velocity (mm/s)†	965 ± 20^{A}	697 ± 30^{B}	749 ± 25^{B}
Aortic Velocity Time Integral (cm)†	3.3 ± 0.1^{A}	2.1 ± 0.1^{B}	2.3 ± 0.1^{B}
Endocardial Ejection Fraction (%)†	54 ± 1^{A}	46 ± 1^{B}	51 ± 1^{A}
Endocardial Fractional Area Change (%)†	40 ± 1^{A}	33 ± 1^{B}	37 ± 1^{A}
M-Mode LV Fractional Shortening (%)†	32 ± 0.6^{A}	27 ± 0.5^{B}	29 ± 0.5^{C}
M-Mode LV Ejection Fraction (%)†	60 ± 1^{A}	53 ± 1^{B}	57 ± 1^{C}

†$P < 0.0001$ comparing measurements from 3 different groups at the same age using one-way ANOVA.
(A)–(C) Mean values with the same letters are not significantly different ($P > 0.05$) by Tukey's multiple comparisons.

efficiently inhibit immune responses mediated by TLR7 and 9 *in vitro* and *in vivo* (13,14). We have evaluated the efficacy of an antagonist of TLR7 and -9 and found a significant reduction in inflammation and serum CK levels, suggesting that blocking this pathway *in vivo* in dystrophin-deficient skeletal muscle could be effective in blocking inflammation. More specifically, IFN-γ gene expression levels of IFN-γ in were significantly decreased in the whole muscle (muscle + immune cells) upon blocking with TLR7/8 antagonist. Furthermore, the increased gene expression of IL-1β in mdx muscle is also reduced upon treatment with TLR7/8 antagonist but this difference did not reach statistical significance. These gene expression data indicate that TLR7/8 antagonists specifically decrease IFN-γ, IL-1β but not TNF-α and TGF-β, suggesting some degree of specificity for TLR antagonists toward certain pro-inflammatory cytokines. It is puzzling to a certain level that the blockage of TLR7/9 reduces muscle damage and pathology in young mdx, but not the absence of myd88. In the double-deficient mice, it is possible that the absence of TLR signaling from birth and the overwhelming nature of early muscle necrosis that spontaneously occurs in mdx mice might induce myd88-independent innate immune mechanisms that are detrimental to skeletal muscle.

Our data suggest that dystrophin-deficient cells undergoing necrosis can release danger signals and trigger an immune inflammatory response by binding to and stimulating innate immune receptors: the so-called 'danger model' of the immune response. This stimulation can activate intracellular signaling pathways, leading not only to an inflammatory response but also to many other effects on dystrophic skeletal muscle. We propose that leaky dystrophin-deficient skeletal muscle releases endogenous danger signals (e.g. ssRNA, S100 proteins and nucleic acids), and that these molecules in turn bind to their respective TLRs or nucleotide receptors on muscle and immune cells and activate downstream processes that facilitate degeneration and regeneration in dystrophic skeletal muscle. Therefore, blocking this pathway may have important therapeutic implications for DMD.

MATERIALS AND METHODS

Mice

Male C57BL/10ScSn-Dmdmdx/J (*mdx*) and C57BL/10ScSnJ mice were purchased from The Jackson Laboratory (Bar Harbor, ME, USA). All experiments were done according to the Institutional Animal Care and Use Committee-approved experimental procedures. Myd88$^{-/-}$ mice were generously provided by Dr Shizuo Akira's group (Osaka University, Osaka, Japan) and maintained in our barrier facility. They were crossed with *mdx* for several generations to produce dystrophin$^{-/-}$/myd88$^{-/-}$ (*mdx*/myd88$^{-/-}$) double-deficient mice. We developed a single nucleotide polymorphism (SNP) based genotyping procedure to identify double-deficient mice in these crosses (Supplementary Material, Fig. S2A and B). Myd88 deficiency was confirmed by both RT-polymerase chain reaction (PCR) and western blotting (Supplementary Material, Fig. S2A and C).

Generation and screening of *mdx*/myd88$^{-/-}$ double-deficient mice

A custom SNP assay for *mdx* genotyping was designed using the Assays-by-Design service (Applied Biosystems, Foster City, CA). The PCR reaction mix contained 3 μl of template DNA at indicated concentrations, 0.4 μl of 20X assay mix, 4 μl of Taqman Genotyping Master Mix (Applied Biosystems) and 0.6 μl of ultrapure water. The assay mix contained the forward primer 5′-GGGAAATTACAGGCTCTGCAAAG-3′ and reverse primer 5′-CATCTCCTTCACAGTGTCACTCA -3′; the fluorescent dye-labeled probes were the VIC®-conjugated wild-type probe, AAGCCATTTT**G**TTGCTCT, and FAM™-conjugated mutant probe, AAGCCATTTT**A**TTGCTCT. Genomic DNA was extracted using the DNeasy Blood and Tissue Kit (Qiagen, Inc., Hilden, Germany) from blood obtained by tail biopsy. Reactions were performed in 96-well PCR plates assembled on ice and centrifuged briefly prior to PCR. PCR was performed according to the manufacturer's instructions, and allelic discrimination was performed on the ABI 7900HT Fast Real-Time PCR System (Applied Biosystems) according to the manufacturer's instructions. Supplementary Material, Figure S2B, shows the separation of the possible genotypes, with homozygous males and homozygous *mdx* females (blue circles), heterozygous females (green circle) and wild-type males and females (red circles). We tested various concentrations of template DNA (0.1–50 ng) and found the clearest separation of the three genotypes with concentrations from 1 to 5 ng. Data obtained from three independent replicates produced consistent allelic discrimination, indicating that SNP analysis is a reliable and reproducible method for genotyping *mdx* mice.

Reagents

The following reagents were used: non-viral synthetic UG-rich ssRNA (ORN06) (Invivogen, San Diego, CA, USA), LPS (Sigma), hyaluronic acid fragments (Alexis Biochemicals, Farmingdale, NY, USA), HMGB1 (eBioscience, San Diego, CA, USA), Alexa Fluor 647-conjugated anti-TLR1 (eBioscience), Alexa Fluor 647-conjugated anti-TLR2 (eBioscience), Alexa Fluor 647-conjugated anti-TLR3 (Imgenex, San Diego, CA, USA), PE-conjugated anti-TLR4 (eBioscience), PE-conjugated anti-TLR7, anti-TLR8 and anti-TLR9 (all from Imgenex),

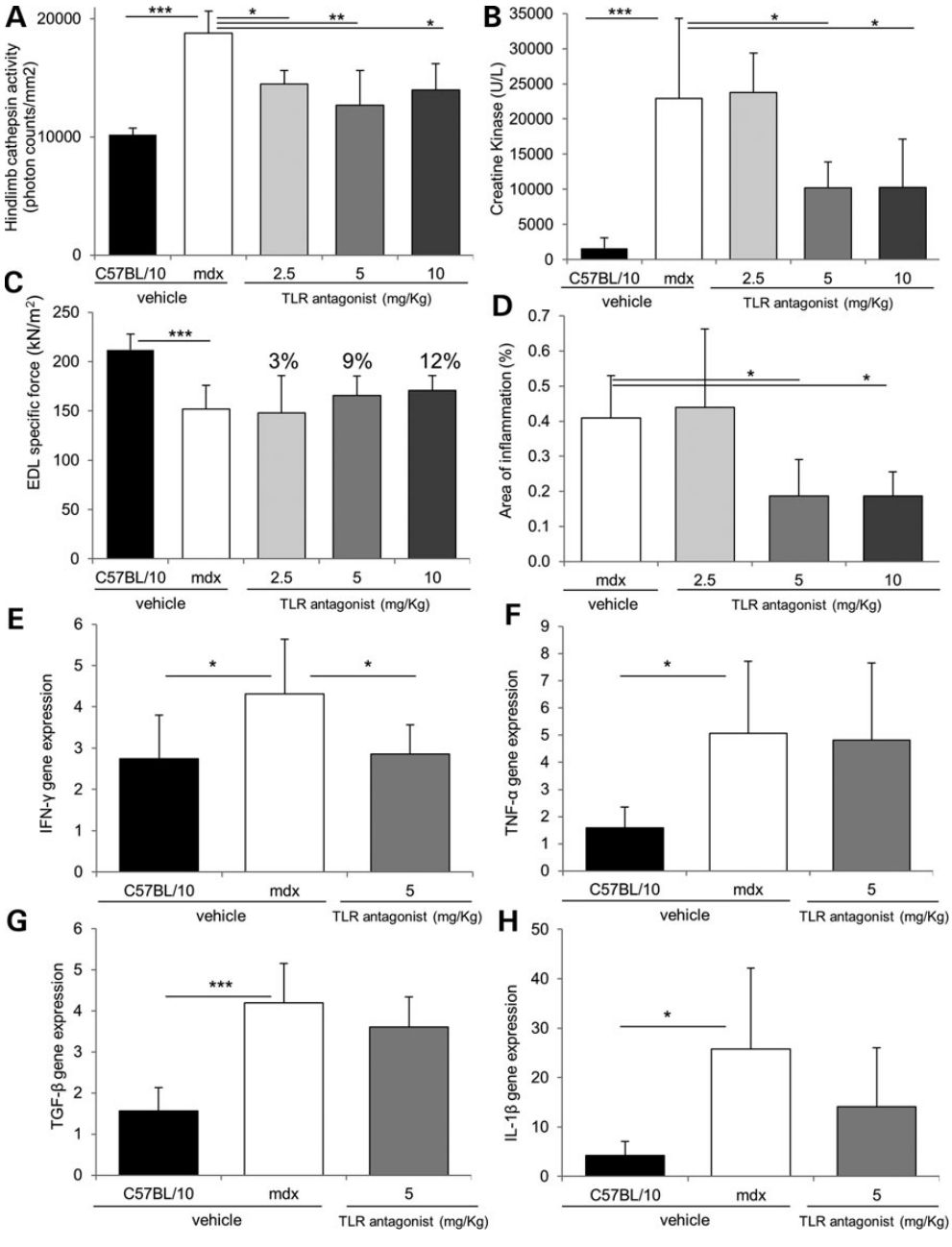

Figure 7. *In vivo* treatment using TLR antagonist ameliorated dystrophic phenotype: C57BL/10 and *mdx* mice (5 weeks old) were treated with PBS or TLR7/8/9 antagonist for 4 weeks (dissolved in PBS for intraperitoneal injection at 2.5, 5 or 10 mg/kg) twice a week. (**A**) Optical imaging for cathepsin activity was performed at high resolution (1.0 mm) in the hindlimb muscles of C57BL/10 and *mdx* vehicle-treated mice and TLR antagonist-treated *mdx* mice. (**B**) Serum creatine kinase activity was evaluated according to manufacturer's instructions. (**C**) Specific force (kN/m^2) produced by EDL muscle was shown. (**D**) Area of inflammation (%) in vehicle and TLR antagonist-treated mdx mice as monitored by H&E staining. (**E**–**H**) Expression of various inflammatory cytokine transcripts in control and mdx groups (vehicle and 5 mg/kg TLR antagonist) as monitored by qPCR ($^*P < 0.05$, $^{**}P < 0.01$ and $^{***}P < 0.001$).

anti-embryonic myosin (The Developmental Studies Hybridoma Bank, Iowa City, IA, USA), TRITC-conjugated anti-desmin, fluorescein isothiocyanate (FITC)-conjugated anti-IgG1 (both from Zymed, Carlsbad, CA), Alexa Fluor 647-conjugated anti-rabbit (Invitrogen, Grand Island, NY, USA), horseradish peroxidase (HRP)-conjugated anti-rabbit, HRP-conjugated anti-mouse (both from Zymed), anti-myogenin, anti-MyoD, HRP-conjugated anti-mouse vinculin (all from Abcam, Cambridge, MA, USA), anti-Pax7 (Developmental Studies Hybridoma Bank), anti-laminin (Sigma), anti-Ki67 (Leica Microsystems, Inc., Buffalo Grove, IL, USA) and biotinylated anti-BrdU (Life Technologies, Grand Island, NY, USA). All antibodies were monoclonals against murine molecules.

Quantification of fibrosis

Paraffin sections of cardiac muscle were stained with Sirius Red (Sigma-Aldrich, St. Louis, MO, USA) and counterstained with hematoxylin. The samples were digitally imaged under a light microscope using a 4× objective and computer software

(Olympus C.A.S.T. Stereology System, Olympus America, Inc., Center Valley, PA, USA). The digital images were processed using Image J (NIH), with an additional threshold color plug-in to process .jpeg images. The percentage of fibrotic area was compared with the total area of the tissue section, and the results were expressed as percent fibrosis for each group.

Myoblast culture and *in vitro* incubation with TLR agonists

All media, reagents and materials were LPS-free, and tissue was carefully handled to prevent contamination with pathogen associated molecular patterns (PAMPs). Diaphragm fragments of 0.5 mm^2 were obtained using tweezers covered with LPS-free pipette tips and surgical blades, then extensively washed in phosphate-buffered saline (PBS) (Sigma-Aldrich, Saint Louis, MO, USA). One or two fragments per well were left overnight in culture in a 48-well plate in complete medium [DMEM high glucose, with 20% fetal calf serum (FCS), 2 mM L-glutamine, 6% chick embryo extract, 100 U penicillin/100 μg streptomycin and 1 mM sodium pyruvate] (all components purchased from Gibco (Carlsbad, CA, USA). After 24 h, the fragments were transferred to new wells for 3 days and assessed for cell death using the *in situ* Cell Death Detection Kit (Roche Applied Science, Indianapolis, IN, USA) according to the manufacturer's instructions, to ensure against any endogenous release of DAMPs from apoptotic cells. The medium was changed every 48 h, and only wells with ≥95% enrichment of myoblasts were maintained in culture until subconfluent (60%). The cells were detached using ice-cold PBS/10 mM ethylenediamine tetraacetic acid (EDTA) (Gibco), incubated for 10 min at 4°C, pooled, washed twice with DMEM/10% FCS, transferred to 8 cm^2 Petri dishes (Corning, Lowell, MA, USA) in complete medium, and cultured until subconfluent. The cultures contained <5% fibroblasts, as evaluated by immunostaining for desmin. The cells were then detached again and transferred to 21 cm^2 Petri dishes (second passage—P2). After they reached sub-confluence, they were detached, and 3×10^4 cells per well (P3) were plated in a 24-well plate and cultured for 24 h. The supernatants were then removed, and the cells were incubated with LPS, ssRNA, HMGB1 or hyaluronic acid fragments in 200 μl of complete medium, at the concentrations indicated in the figure legends, for 18 h. Secretion of cytokines (TNF, IL-12p70, IL-6, IFN-γ, IL-10 and MCP1) was evaluated in supernatants by flow cytometry using the inflammatory CBA kit (BD, San Jose, CA, USA) as recommended by the manufacturer. The upper limit of the standard curve was 5000 pg/ml.

In vivo injection of TLR ligands

ssRNA (9 or 12 μg/ml) or LPS (2 μg/ml) was administered as four injections of 10 μl per quadriceps muscle into 2-month-old *mdx* and C57BL/10 mice ($n = 5$ mice/group). Saline was similarly injected into the contralateral quadriceps as a negative control. The mice were treated a total of three times (four injections per muscle each time) at 3-day intervals, and all mice were euthanized for tissue collection 3 days after the last injection.

Histopathology and immunohistochemistry

For H&E staining and immunohistochemical labeling, the diaphragm, gastrocnemius and quadriceps muscles were removed, frozen using isopentane chilled in liquid nitrogen and kept at −80°C until used. For immunofluorescent staining, 10 μm frozen sections were fixed with 2% paraformaldehyde for 10 min at room temperature. For eMHC labeling, we used unfixed tissue sections, and any endogenous peroxidase in the samples was blocked using 3% H_2O_2 for 10 min. The samples were then incubated with FcγR blocking solution (DMEM with 10% FCS and 10% normal sheep serum) and washed twice with PBS before overnight incubation at room temperature with previously titrated primary antibodies. The samples were then extensively washed with PBS and incubated with Alexa Fluor 488-conjugated anti-mouse (for MyoD), Alexa Fluor 647-conjugated anti-rabbit (for myogenin), HRP-conjugated anti-mouse (for eMHC), or Alexa Fluor 488-conjugated anti-rabbit or Alexa Fluor 568-conjugated anti-mouse (for Ki67, Pax7 and MyoD). For immunofluorescent staining, glass slides were mounted using ProLong® Gold anti-fading reagent with DAPI (Invitrogen), and eMHC labeling was revealed using 3-amino-9-ethylcarbazole (AEC) (Dako, Carpinteria, CA). Quantification of $eMHC^+$ cells was done in ≥60 microscopic fields per muscle and age group, in at least three mice per group, and only dark-brown cells were considered positive.

For evaluating the degenerating fibers, frozen sections were fixed in ethanol, rinsed and incubated (for 30 min at 20°C) with blocking solution (PBS, 2% BSA, 0.5% Triton X-100, 0.1% Tween 20, 20% sheep serum). Samples were washed and incubated with IgM overnight at 4°C, washed and incubated for 60 min (20°C) with the appropriate secondary antibody and Hoechst 33342 (9.0 μM, 10 min) and analyzed as described previously (15).

Bromodeoxyuridine (brdU) staining

Bromodeoxyuridine (Sigma, 0.8 mg/ml) was administered to 4-month-old mice (three animals per group) in the drinking water for 1 week and the tissues were harvested 1-week after treatment. Animals were then sacrificed and gastrocnemius and diaphragm muscles were flash-frozen, then sectioned. Sections were fixed in ice-cold acetone for 10 min, denatured in 2N HCl for 1 h, washed with 0.1% Tween-20 in 1X Tris-buffered saline (TBS-T) (pH 7.4) and neutralized with 0.15 M sodium borate. Sections were blocked for 1 h with a solution containing 20% normal goat serum (Vector Labs), 20% bovine serum albumin, 0.5% Triton X-100 and 0.1% Tween, and then incubated overnight with blocking solution containing anti-BrdU and anti-laminin antibodies. The following day, sections were washed with TBS-T then incubated with blocking solution containing FITC-conjugated anti-streptavidin, Alexa Fluor 633-conjugated goat anti-rabbit antibody and propidium iodide. Sections were imaged using a Zeiss Axiovert fluorescent microscope, and BrdU-positive cells were quantitated using the ImageJ software ($n = 3$ sections per muscle).

Flow cytometry

Diaphragm, soleus and gastrocnemius muscles were collected from 2 to 4-week-old *mdx*, *mdx*/myd88$^{-/-}$ and mdx/myd88$^{+/+}$ mice, extensively washed in ice-cold PBS, and cut into 1–2-mm fragments. These fragments were transferred to RPMI 1640 (Gibco) containing collagenase type IA (0.01%)

(Sigma) and incubated for 30–40 min at 37°C under gentle agitation. Isolated cells were washed twice in RPMI 1640 and incubated for 30 min at 4°C in FcγR blocking solution. They were then incubated with anti-membrane TLR monoclonal antibodies for 30 min on ice, washed twice using RPMI/10% FCS, incubated with Fixperm 2 Solution (BD Biosciences) as recommended by the manufacturer, and washed with PBS. Intracellular labeling was done for TLRs (3, 7–9) and MyoD; all antibodies used were previously titrated for optimal labeling of cells. After 30 min incubation at room temperature, the samples were washed in PBS, post-fixed using 2% formaldehyde, and analyzed using a FACSCalibur™ flow cytometer (BD). Data analysis was performed using Summit software version 4.3 (Dako). Flow cytometry for BrdU was performed using the FITC BrdU Flow Kit as recommended by the manufacturer (BD Biosciences).

Western blotting

Total proteins from diaphragm and gastrocnemius skeletal muscle extracts were obtained using extraction buffer (50 mM Tris–HCl, with NP-40 1%, 1 mM leupeptin, 100 mM phenylmethylsulfonyl fluoride, 1 mM pepstatin A and 100 mM EDTA, all purchased from Sigma). Proteins (50 μg per lane) were resolved on a 4–12% Bis-Tris sodium dodecyl sulfate polyacrylamide gel electrophoresis (sodium dodecyl sulfate–polyacrylamide gel electrophoresis) gradient gel (Invitrogen). Proteins were transferred to nitrocellulose membranes, blocked using 5% non-fat dry milk in TBS-T buffer, and incubated with anti-MyoD, anti-myd88, or anti-myogenin antibody for 3 h. The membranes were then washed with TBS-T buffer and incubated with HRP-conjugated anti-mouse or HRP-conjugated anti-rabbit secondary antibody for 1 h at room temperature. Following another series of washes, blots were incubated for 1 min using enhanced chemi-luminesence (Amersham, Piscataway, NJ, USA), and autoradiograms were scanned as described earlier. To assess equal gel loading, membranes were stripped using a stripping buffer (Thermo Scientific, Rockford, IL, USA) for 30 min at 50°C, relabeled with an anti-vinculin antibody, and visualized as described previously (2,16,17).

High-frequency echocardiography

Echocardiography (VisualSonics Vevo 770, Toronto, Canada) was performed in 10–12-month-old *mdx*/myd88$^{+/+}$, *mdx*/myd88$^{-/-}$ and control (C57BL/10xC57BL/6) mice. All mice were first anesthetized with 5% isoflurane mixed with 100% oxygen at a flow rate of 0.6 l/min, then maintained under anesthesia with a 1.5% isoflurane/oxygen flow. A heating lamp was used to keep the heart rate and temperature constant at physiological status. Heart rate and aortic velocity from the Doppler image, FS and EF from the M-mode image, and the endocardial EF and FAC from 2D electrocardiogram-gated kilohertz visualization (EKV) image were obtained for cardiac function assessment. Qualitative and quantitative measurements were made offline using the analytic software. Means and standard errors (SEs) were calculated for all ultrasound parameters, and statistical analysis was carried out using analysis of variance (ANOVA) and Tukey's multiple comparisons.

Synthesis and purification of antagonist compound

The antagonist compound, 5′-CAATCTGUC*G1TTCACTGU-3′ (C* is 5′-methyl-dC, G* is 7-deaza-dG, underlined nucleotides are 2′-*O*-methyl-ribonucleotides, and all other nucleotides are 2′-deoxynucleotides) was synthesized with a phosphorothioate backbone at Idera Pharmaceuticals as described previously (6). The antagonist was purified on anion-exchange high pressure (or high performance) liquid chromatography (HPLC) and characterized by capillary gel electrophoresis (CGE), anion-exchange and reverse-phase HPLCs and matrix-assisted laser desorption/ionization-time of flight mass spectrometry to assess purity and molecular mass. The purity of the full-length oligonucleotide ranged from 98 to 99%, and it contained <0.075 EU/mg of endotoxin by the *Limulus* assay (Bio-Whittaker).

Effect of the TLR7/9 antagonist on disease phenotype in *mdx* mice

The protocol was approved, and all mice were handled according to the local Institutional Animal Care and Use Committee guidelines. *mdx* and C57BL/10 male mice were purchased from the Jackson Laboratory (Bar Harbor) at 4 weeks of age and were allowed to acclimate to the room before the trial started. All mice were housed in individually vented cage systems on a 12 h light–dark cycle and received standard mouse chow and purified water *ad libitum*. Mice were weighed once a week, and the animals were randomized on the basis of body weight. This study was conducted in a blinded fashion, with treatment begun when the mice were 5 weeks of age. All mice were first acclimated to the various instruments used for functional testing. The TLR7/9 antagonist was dissolved in PBS, and 150 μl was injected intraperitoneally at three different dosages (2.5, 5 and 10 mg/kg) twice a week. PBS was injected into control groups. In total, there were five groups of eight age-matched male mice each: (i) untreated C57BL/10 mice (vehicle control); (ii) untreated *mdx* mice (vehicle control); (iii) *mdx* mice receiving 2.5 mg/kg TLR7/9 antagonist; (iv) *mdx* mice receiving 5 mg/kg antagonist; and (v) *mdx* mice receiving 10 mg/kg antagonist. Grip strength tests and optical imaging for cathepsin activity were performed after 4 weeks of treatment, when the mice were 9 weeks old. After 5 weeks of treatment (10-week-old mice), blood and tissue samples were harvested from the mice, and *in vitro* muscle force, serum creatine kinase, and histological data were collected. All the tests were conducted as described previously (18–21).

Assessment of inflammatory cytokine gene expression

Expression of inflammatory cytokine transcripts (IFN-γ TNF-α, TGF-β and IL-1β) was monitored using by RT-PCR. Gastrocnemius muscles were obtained from C57BL/10, vehicle-treated *mdx*, and 5 mg/kg antagonist-treated *mdx* mice, and RNA were isolated using TRIzol reagent (Life Technologies) according to the manufacturer's protocol. One microgram of total RNA was reverse transcribed using a High Capacity cDNA Reverse Transcription kit (Invitrogen). Quantitative real-time PCR was performed using the StepOnePlus™ PCR system and the relative quantity of gene expression was calculated using

hypoxanthine phosphoribosyl transferase (HPRT) as an endogenous control by the StepOne™ software v2.0. Primer probe sets, purchased from Life Technologies/Invitrogen, were as follows: IL-1β, Mm00434228_m1; TNF-α, Mm00443258_m1; MCP-1(CCL2), Mm00441242_m1; IFN-γ, Mm01168134_ml; TGF-β1, Mm01178819_m1; HPRT, Mm01545399_m1. The relative expression of each transcript was calculated based on the expression of HPRT gene, and relative fold changes were represented as means ± SE.

Statistical analysis

Except where indicated, data were statistically evaluated using Student's *t*-test, and *P*-values ≤ 0.05 were regarded as significant. Mean comparisons between treatment groups were done using ANOVA. For those ANOVA models showing a significant overall *P*-value ($P < 0.01$), Tukey's multiple comparison tests were performed, with the resulting *P*-values adjusted for multiple testing. Individual data above or below two standard deviations were excluded.

SUPPLEMENTARY MATERIAL

Supplementary Material is available at *HMG* Online.

ACKNOWLEDGMENTS

The authors thank Dr Deborah McClellan for editing this manuscript.

Conflict of Interest statement. D.W., W.J. and S.A. are employees and E.R.K. was an exemployee of Idera Pharmaceuticals and hold stock options.

FUNDING

This work was partially supported by National Institutes of Health (NIH) IDDRC grant P30HD40677 and partially supported by NIH core grants NCMRR/NINDS 2R24HD050846-06 (National Center for Medical Rehabilitation Research) and IDDRC 5P30HD040677-10 (Intellectual and Developmental Disabilities Research Center) and by NIH NCRR UL1RR031988 (GWU-CNMC CTSI). Dr Nagaraju is supported by NIH (RO1-AR050478, 5U54HD053177 and K26OD011171), the Muscular Dystrophy Association (1P50AR060836-01) and the US Department of Defense (W81XWH-05-1-0616 and W81XWH-11-1-0782).

REFERENCES

1. Chen, Y.W., Nagaraju, K., Bakay, M., McIntyre, O., Rawat, R., Shi, R. and Hoffman, E.P. (2005) Early onset of inflammation and later involvement of TGFbeta in Duchenne muscular dystrophy. *Neurology*, **65**, 826–834.
2. Rawat, R., Cohen, T.V., Ampong, B., Francia, D., Henriques-Pons, A., Hoffman, E.P. and Nagaraju, K. (2010) Inflammasome up-regulation and activation in dysferlin-deficient skeletal muscle. *Am. J. Pathol.*, **176**, 2891–2900.
3. Matzinger, P. (2002) An innate sense of danger. *Ann. N. Y. Acad Sci*, **961**, 341–342.
4. Matzinger, P. (1998) An innate sense of danger. *Semin Immunol*, **10**, 399–415.
5. O'Neill, L.A. (2003) The role of MyD88-like adapters in Toll-like receptor signal transduction. *Biochem Soc Trans*, **31**, 643–647.
6. Kandimalla, E.R., Bhagat, L., Wang, D., Yu, D., Sullivan, T., La Monica, N. and Agrawal, S. (2013) Design, synthesis and biological evaluation of novel antagonist compounds of Toll-like receptors 7, 8 and 9. *Nucleic Acids Res.*, **41**, 3947–3961.
7. Ohashi, K., Burkart, V., Flohe, S. and Kolb, H. (2000) Cutting edge: heat shock protein 60 is a putative endogenous ligand of the toll-like receptor-4 complex. *J. Immunol.*, **164**, 558–561.
8. Langen, R.C., Schols, A.M., Kelders, M.C., Van Der Velden, J.L., Wouters, E.F. and Janssen-Heininger, Y.M. (2002) Tumor necrosis factor-alpha inhibits myogenesis through redox-dependent and -independent pathways. *Am. J. Physiol.. Cell Physiology*, **283**, C714–C721.
9. Odegaard, J.I., Ricardo-Gonzalez, R.R., Goforth, M.H., Morel, C.R., Subramanian, V., Mukundan, L., Red Eagle, A., Vats, D., Brombacher, F., Ferrante, A.W. *et al.* (2007) Macrophage-specific PPARgamma controls alternative activation and improves insulin resistance. *Nature*, **447**, 1116–1120.
10. Arslan, F., de Kleijn, D.P. and Pasterkamp, G. (2011) Innate immune signaling in cardiac ischemia. *Nat. Rev. Cardiol.*, **8**, 292–300.
11. Blyszczuk, P., Kania, G., Dieterle, T., Marty, R.R., Valaperti, A., Berthonneche, C., Pedrazzini, T., Berger, C.T., Dirnhofer, S., Matter, C.M. *et al.* (2009) Myeloid differentiation factor-88/interleukin-1 signaling controls cardiac fibrosis and heart failure progression in inflammatory dilated cardiomyopathy. *Circ. Res.*, **105**, 912–920.
12. Van Tassell, B.W., Seropian, I.M., Toldo, S., Salloum, F.N., Smithson, L., Varma, A., Hoke, N.N., Gelwix, C., Chau, V. and Abbate, A. (2010) Pharmacologic inhibition of myeloid differentiation factor 88 (MyD88) prevents left ventricular dilation and hypertrophy after experimental acute myocardial infarction in the mouse. *J. Cardiovasc. Pharmacol.*, **55**, 385–390.
13. Wang, D., Bhagat, L., Yu, D., Zhu, F.G., Tang, J.X., Kandimalla, E.R. and Agrawal, S. (2009) Oligodeoxyribonucleotide-based antagonists for Toll-like receptors 7 and 9. *J. Med. Chem.*, **52**, 551–558.
14. Yu, D., Wang, D., Zhu, F.G., Bhagat, L., Dai, M., Kandimalla, E.R. and Agrawal, S. (2009) Modifications incorporated in CpG motifs of oligodeoxynucleotides lead to antagonist activity of toll-like receptors 7 and 9. *J. Med. Chem.*, **52**, 5108–5114.
15. Jahnke, V.E., Van Der Meulen, J.H., Johnston, H.K., Ghimbovschi, S., Partridge, T., Hoffman, E.P. and Nagaraju, K. (2012) Metabolic remodeling agents show beneficial effects in the dystrophin-deficient mdx mouse model. *Skelet. Muscle*, **2**, 16.
16. Rayavarapu, S., Coley, W., Van der Meulen, J.H., Cakir, E., Tappeta, K., Kinder, T.B., Dillingham, B., Brown, K.J., Hathout, Y. and Nagaraju, K. (2013) Activation of the ubiquitin proteasome pathway in a mouse model of inflammatory myopathy: a potential therapeutic target. *Arthritis Rheum.*, **65**, 3248–3258.
17. Rayavarapu, S., Coley, W., Cakir, E., Jahnke, V., Takeda, S., Aoki, Y., Grodish-Dressman, H., Jaiswal, J.K., Hoffman, E.P., Brown, K.J. *et al.* (2013) Identification of disease specific pathways using in vivo SILAC proteomics in dystrophin deficient mdx mouse. *Mol. Cell. Proteom.*, **12**, 1061–1073.
18. Spurney, C.F., Gordish-Dressman, H., Guerron, A.D., Sali, A., Pandey, G.S., Rawat, R., Van Der Meulen, J.H., Cha, H.J., Pistilli, E.E., Partridge, T.A. *et al.* (2009) Preclinical drug trials in the mdx mouse: assessment of reliable and sensitive outcome measures. *Muscle Nerve*, **39**, 591–602.
19. Rayavarapu, S., Van der Meulen, J.H., Gordish-Dressman, H., Hoffman, E.P., Nagaraju, K. and Knoblach, S.M. (2010) Characterization of dysferlin deficient SJL/J mice to assess preclinical drug efficacy: fasudil exacerbates muscle disease phenotype. *PloS One*, **5**, e12981.
20. Coley, W., Rayavarapu, S., Pandey, G.S., Sabina, R.L., Van der Meulen, J.H., Ampong, B., Wortmann, R.L., Rawat, R. and Nagaraju, K. (2012) The molecular basis of skeletal muscle weakness in a mouse model of inflammatory myopathy. *Arthritis Rheum*, **64**, 3750–3759.
21. Coley, W., Rayavarapu, S., van der Meulen, J.H., Duba, A.S. and Nagaraju, K. (2013) Daily supplementation of D-ribose shows no therapeutic benefits in the MHC-I transgenic mouse model of inflammatory myositis. *PloS One*, **8**, e65970.